The following article appeared in Optics Express 23(11): 14380-14390 (2015); and may be found at: https://doi.org/10.1364/OE.23.014380

Removing lateral chromatic aberration in bright field optical microscopy

Miguel Guzmán-Altamirano[1,2] and Braulio Gutiérrez-Medina[1,*]

[1]*Advanced Materials Division, Instituto Potosino de Investigación Científica y Tecnológica, San Luis Potosí, San Luis Potosí 78216, Mexico*

[2]*MEMS Department, Instituto Tecnológico Superior de Irapuato, Irapuato, Guanajuato 36500, Mexico*

[*]*bgutierrez@ipicyt.edu.mx*

Abstract: We present an efficient alternative to remove lateral chromatic aberration (LCA) in bright field light microscopy images. Our procedure is based on error calibration using time-sequential acquisition at different wavelengths, and error correction through digital image warping. Measurement of the displacements of fiducial marks in the red and green images relative to blue provide calibration factors that are subsequently used in test images to realign color channels digitally. We demonstrate quantitative improvement in the position and boundaries of objects in target slides and in the color content and morphology of specimens in stained biological samples. Our results show a reduction of LCA content below the 0.1% level.

OCIS codes: (220.1000) Aberration compensation; (100.2000) Digital image processing; (180.0180) Microscopy.

References and links

1. M. Born and E. Wolf, *Principles of Optics, Electromagnetic Theory of Propagation, Interference and Diffraction of Light* (Cambridge University, 2002).
2. E. Hecht, *Optics* (Addison Wesley, 2002).
3. R. G. Willson and S. A. Shafer, "Active lens control for high precision computer imaging," in *Proceedings of IEEE International Conference on Robotics and Automation* (IEEE, 1991), pp. 2063–2070.
4. C. L. Novak, S. A. Shafer, and R. G. Willson, "Obtaining accurate color images for machine-vision research," Proc. SPIE **1250**, 54–68 (1990).
5. T. E. Boult and G. Wolberg, "Correcting chromatic aberrations using image warping," in *Proceedings of IEEE Conference on Computer Vision and Pattern Recognition* (IEEE, 1992), pp. 684–687.
6. C. A. Glasbey and K. V. Mardia, "A review of image-warping methods," J. Appl. Stat. **25**(2), 155–171 (1998).
7. V. Rudakova and P. Monasse, "Precise correction of lateral chromatic aberration in images," in *Image and Video Technology*, R. Klette, M. Rivera, Mariano, S. Satoh, Eds. (Springer, 2014), pp. 12–22.
8. C. Soon-Wook, K. Byoung-Kwang, and S. Woo-Jin, "Detecting and eliminating chromatic aberration in digital images," in *Proceedings of IEEE International Conference on Image Processing* (IEEE, 2009), pp. 3905–3908.
9. C. J. Schuler, M. Hirsch, S. Harmeling, and B. Scholkopf, "Non-stationary correction of optical aberrations," in *Proceedings of IEEE International Conference on Computer Vision* (IEEE, 2011), pp. 659–666.
10. H. Kang, S.-H. Lee, J. Chang, and M. G. Kang, "Partial differential equation–based approach for removal of chromatic aberration with local characteristics," J. Electron. Imaging **19**(3), 033016 (2010).
11. H. E. Keller, "Objective lenses for confocal microscopy," in *Handbook of Biological Confocal Microscopy*, 2ed., J. B. Pawley, ed. (Plenum, New York, 1995). pp. 111–126.
12. S. Fenz, H. Mathée, G. Kreth, D. Baddeley, Y. Weiland, J. Schwarz-Finstlerle, C. G. Cremer, and U. J. Birk, "Two-color intranuclear distance measurements of gene regions in human lymphocytes," Proc. SPIE **6630**, 663002 (2007).
13. N. S. White, R. J. Errington, M. D. Fricker, and J. L. Wood, "Aberration control in quantitative imaging of botanical specimens by multidimensional fluorescence microscopy," J. Microsc. **181**(2), 99–116 (1996).
14. E. M. M. Manders, "Chromatic shift in multicolour confocal microscopy," J. Microsc. **185**(3), 321–328 (1997).
15. M. Kozubek and P. Matula, "An efficient algorithm for measurement and correction of chromatic aberrations in fluorescence microscopy," J. Microsc. **200**(3), 206–217 (2000).
16. S. Tucker, W. T. Cathey, and E. Dowski, Jr., "Extended depth of field and aberration control for inexpensive digital microscope systems," Opt. Express **4**(11), 467–474 (1999).
17. N. A. M. Isa, "Automated edge detection technique for pap smear images using moving K-means clustering and modified seed based region growing algorithm," Int. J. Comput. Int. Manage. **13**, 45–59 (2005).

#235180 - $15.00 USD Received 24 Feb 2015; revised 27 Apr 2015; accepted 27 Apr 2015; published 22 May 2015

18. H. Irshad, A. Veillard, L. Roux, and D. Racoceanu, "Methods for nuclei detection, segmentation, and classification in digital histopathology: A review-current status and future potential," IEEE Rev. Biomed. Eng. **7**, 97–114 (2014).
19. M. P. De Sá-otero, A. González, M. Rodríguez-Damián, and E. Cernadas, "Computer-aided identification of allergenic species of urticaceae pollen," Grana **43**(4), 224–230 (2004).
20. N. R. Nguyen, M. Donalson-Matasci, and M. C. Shin, "Improving pollen classification with less training effort," in *Proceedings of IEEE Workshop on Applications of Computer Vision* (IEEE, 2013), pp. 421–426.
21. B. Hohman, "LED light source: major advance in fluorescence microscopy," Biomed. Instrum. Technol. **41**(6), 461–464 (2007).
22. T. P. Meyrath, "An analog current controller design for laser diodes." *http://atomoptics.uoregon.edu/unilaser/unibody_files/peripherals/protection_circuit/meyrath_03.pdf*.
23. R. Lukac and K. N. Plataniotis, "Normalized color-ratio modeling for CFA interpolation," IEEE Trans. Consum. Electron. **50**(2), 737–745 (2004).
24. R. Ramanath, W. E. Snyder, G. L. Bilbro, and I. I. I. W. A. Sander, "Demosaicking methods for bayer color arrays," J. Electron. Imaging **11**(3), 306–315 (2002).
25. M. Singh and T. Singh, "Joint chromatic aberration correction and demosaicking," Proc. SPIE **8299**, 82990D (2012).
26. J. Parker, R. V. Kenyon, and D. E. Troxel, "Comparison of interpolating methods for image resampling," IEEE Trans. Med. Imaging **2**(1), 31–39 (1983).
27. M. T. Orchard and C. A. Bouman, "Color quantization of images," IEEE T. Signal Process. **39**, 2677–2690 (1991).
28. J. Mallon and P. F. Whelan, "Calibration and removal of lateral chromatic aberration in images," Pattern Recognit. Lett. **28**(1), 125–135 (2007).
29. MATLAB R2014b documentation, "Detect and measure circular objects in an image," (Mathworks, 2014), *http://www.mathworks.com/help/images/examples/detect-and-measure-circular-objects-in-an-image.html*.
30. MATLAB R2014b documentation, "Granulometry of snowflakes," (Mathworks, 2014), *http://www.mathworks.com/help/images/examples/granulometry-of-snowflakes.html*.
31. R. S. Montero and E. Bribiesca, "State of the art of compactness and circularity measures," Int. Math. Forum **4**, 1305–1335 (2009).
32. K. A. Holt and M. S. Bebbington, "Separating morphologically similar pollen types using basic shape features from digital images: A preliminary study(1.)," Appl. Plant Sci. **2**(8), 1400032 (2014).
33. S. J. Mudd and H. S. Arathi, "Image analysis protocol for detecting and counting viable and inviable pollen grains," J. Plant Stud. **1**, 158–167 (2012).

1. Introduction

Optical imaging systems produce outputs that are blurred and distorted due to a number of aberrations derived from the intrinsic properties of these systems. Lateral chromatic aberration (LCA) [1], the wavelength-dependent focus at different positions in the image plane, has traditionally been corrected by introducing compensating material dispersion through additional elements in the optical train [2]. However, a number of considerations such as reduction of cost, the need for corrections to an increasing degree, or the convenience of using aberration-prone, low-grade optical materials (e.g. plastic) have motivated the search for alternatives to remove chromatic aberration. The most widely used approach in this quest has been digital image processing, although hybrid optical-digital methods for controlling chromatic alterations have also been developed [3].

In the context of digital image recording, LCA leads to relative displacements among the corresponding pixels of the red, green and blue (RGB) channels [4]. Two main consequences arise: the measurable variables that depend on pixel (px) positions are captured incorrectly, and the apparition of color hue shifts at the edges of objects in images affects proper characterization of morphology, boundaries and color content [5]. To remedy these errors, a global image warping method has been proposed, consisting of two main steps [6]. First, the optical system is calibrated where one or more high-contrast captured images are used to determine the parameters that characterize the degree of deviation in pixel positions among the different color channels. In the second stage, the calibration parameters are used to realign color channels digitally (warping) [7]. Alternatively, correction methods based on edge gradient detection [8], point spread function deconvolution [9], and analytic modeling [10], have been developed.

#235180 - $15.00 USD Received 24 Feb 2015; revised 27 Apr 2015; accepted 27 Apr 2015; published 22 May 2015

In the field of optical microscopy, the modern fluorescence microscope objectives bring on a high correction factor for chromatic aberration, admitting errors only at the ~0.2% level [11]. Nevertheless, this value may not be enough in many applications, particularly where measurements of position variables in the sub-pixel range are required [12–14]. In one example, where further corrections to chromatic aberration in the fluorescence microscope have been implemented, Kozubek and Matula [15] first imaged multiply-labeled microspheres and obtained the displacement factors between misaligned color channels. Then, these factors were used to warp two color channels to a reference color channel, reducing the magnitude of chromatic aberration from ~240 nm to ~10 nm laterally and from ~300 nm to ~60 nm axially. This efficient procedure is relatively straightforward, and has been successfully applied (e.g. in studies where the precision in measurements of distance between two labeled gene regions was improved [12]).

In contrast, for bright field microscopy only a few developments have been realized to further remove chromatic aberration beyond what is achieved by the microscope objective. Tucker *et al.* report the use of digital processing in conjunction with a phase mask to extend the depth of field or focus and provide control over axial chromatic aberration [16]. Although it has received less attention compared to the case of fluorescence, the improvement of the imaging in bright field microscopy is of great interest, notably in the analysis of biological samples. For instance, accurate assessments of image features like borders, textures and color content are required in histological analyses for reliable evaluations of sample tissue [17, 18]. Particle classification studies often require aberration-free images as well [19, 20].

Here, we devise and apply an image warping strategy to remove LCA content in bright field optical microscopy images. Using a modified low-cost microscope, we capture sequential images of polystyrene microspheres under illumination at different wavelengths, and obtain the corresponding centroids in the different color channels. After this calibration step, where the magnitude of the LCA is determined over the entire field of view, we use the calibration constants found to remove LCA through digital image warping [15]. We validate quantitatively our method by analyzing borders and distances in a USAF 1951 chart image, and by comparing the color content and morphology of specimens in stained biological samples before and after correction. The results show a significant improvement in the quantitative parameters evaluated and the reduction of LCA-related errors below the 0.1% level.

2. Experimental setup

The general scheme of our methodology to remove LCA is shown in Fig. 1(a). After a LCA calibration step (not shown, described in Section 3.1), a given image under white (***W***) illumination is separated into the red (***R***), green (***G***) and blue (***B***) image components. We select the ***B*** channel as a reference image for subsequent correction, therefore this channel remains unaltered. We then apply warping to the ***R*** and ***G*** channels, reducing pixel position misalignments with respect to the ***B*** channel. Finally, we use the corrected ***R*** and ***G*** channels together with the original ***B*** channel to rebuild the image, now with LCA removed.

To implement our strategy, we have chosen a generic student-grade microscope (Iroscope, M6-11T) working under bright field. This option provides an opportunity to see how LCA under suboptimal imaging conditions (i.e. non-Koehler illumination, simple plan objectives, lack of a dedicated camera port –see below–) can be reverted through digital warping. The original illumination source of the microscope was replaced by an optical multiplexor, see Fig. 1(b). The light from a high power LED (Multicomp, OSW-8339) featuring three chips at different peak wavelengths (620 nm, 520 nm and 460 nm) and the light from a tungsten lamp were coupled into a single-strand optical guide that merely propagates light and does not form images (liquid light guide, Edmund Scientific, Model No. 53-691, core diameter: 5 mm, numerical aperture: 0.55) by means of a telescope and a beamsplitter, providing us with the possibility of sequential illumination with red, green, blue, and white light. A diffuser lens

#235180 - $15.00 USD Received 24 Feb 2015; revised 27 Apr 2015; accepted 27 Apr 2015; published 22 May 2015

within the field lenses provided homogenous illumination. Stable illumination at ~1 kHz bandwidth was achieved by current feedback control of the LED source [21, 22].

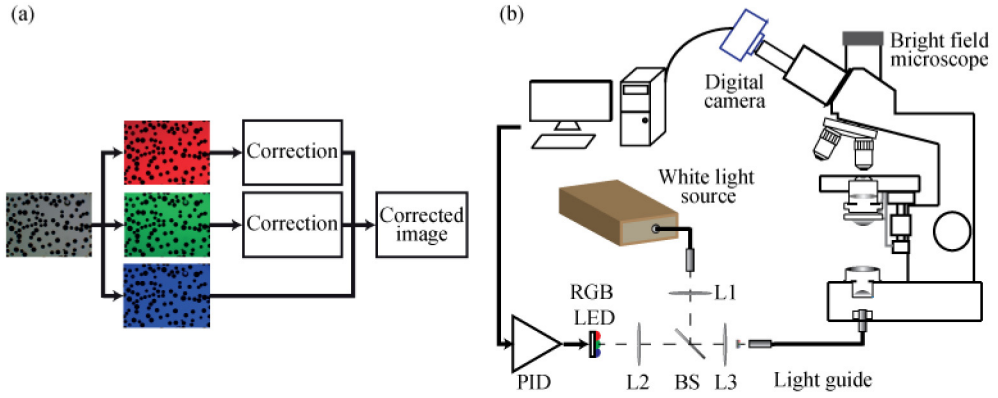

Fig. 1. Approach to remove LCA in bright field microscopy images. (a) Flow chart of image processing. (b) Outline of the experimental setup used. L: lenses, BS: beam splitter, PID: Proportional-Integral-Differential LED current feedback circuit.

Further power on/off and light intensity control of the LED was carried out using a DAQ module (National instruments, NI-9221) managed with LabVIEW routines. To capture images in the binocular microscope, we attached a CMOS camera (AMSCOPE, MU-300, 2048 × 1536 pixels) to one of the eyepieces. All of the work presented here was performed using a 10X objective.

3. Calibration and correction of LCA

3.1. Calibration procedure

To determine the extent of LCA in images, we obtained the position of fiducial marks under illumination at different wavelengths. A test slide was fabricated by fixing polystyrene microspheres with sizes between 40 and 90 um to a microscope slide using transparent mucilage glue (Stafford), resulting in beads randomly distributed. Next, we captured three images of the customized slide using red, green and blue illumination, sequentially, at time intervals of 1 s. This sequential procedure provides a faithful groundwork to probe each camera color channel, as it minimizes negative effects due to color crosstalk [23] and demosaicing [24, 25] during the recording of digital images. For a given captured image its corresponding color channel was extracted, generating a monochromatic version of the image for each (red, green and blue) color channel.

To assess the magnitude of LCA, we first obtained the coordinates (X_i^M, Y_i^M) of the centroid for every *i*-th bead in the field of view, for each channel ($M = R,G,B$). This operation was easily carried out (due to the high contrast of bead images) by: (1) bead discrimination through application of a threshold value, (2) conversion from gray scale to binary scale, and (3) centroid coordinate determination. The amount of LCA is then determined pairwise between different color channels, calculated as the Euclidean distance between the centroids of a given bead in the ***B*** and ***R*** channels (***B-R***): $\Delta X_i^{BR} = X_i^B - X_i^R$, and between the ***B*** and ***G*** channels (***B-G***): $\Delta X_i^{BG} = X_i^B - X_i^G$. These procedures were performed in MATLAB.

The distribution of the magnitude of LCA found in our system is shown in Fig. 2, where both ***B-R*** [Fig. 2(a)] and ***B-G*** [Fig. 2(b)] distances reveal a semi-conic surface that indicates minimal LCA (around the same point in both cases) and linear growth toward the edges of the field of view. A maximal lateral shift in the position of beads of ~12 pixels is observed for the ***B-R*** pair, whereas for ***B-G*** distances a smaller maximal value of ~6 pixels is recorded. A vector representation of the LCA shift is presented in Fig. 2(c) and Fig. 2(d), where it

#235180 - $15.00 USD Received 24 Feb 2015; revised 27 Apr 2015; accepted 27 Apr 2015; published 22 May 2015

becomes clear the radial nature of LCA in our case (this behavior may not always occur; see, for example, reference [15]).

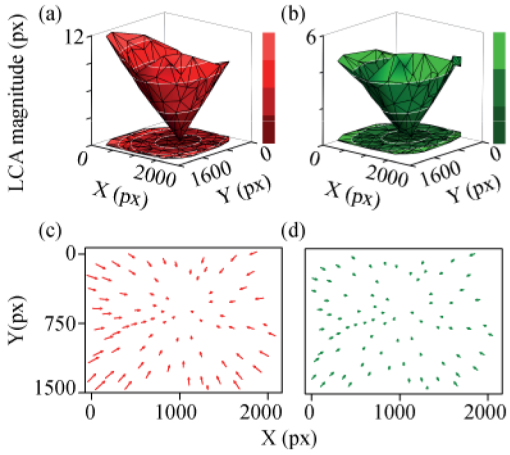

Fig. 2. The measured magnitude of LCA in our microscope. 3D graphs show a linear radial behavior of the magnitude of LCA in both (a) ***B-R*** and (b) ***B-G*** cases. The corresponding vector graphs below show the relative displacements in the positions of the test microspheres between the (c) ***B-R*** and (d) ***B-G*** channels. The magnitude of the vectors in (c)-(d) were magnified by 10 × for clarity.

Plots of ΔX vs. X^B and ΔY vs. Y^B for the ***B-R*** pair are shown in Fig. 3(a) and Fig. 3(b), respectively, whereas Fig. 3(c) and Fig. 3(d) show the corresponding plots for the ***B-G*** pair. All plots were fit to linear functions, from where slopes and x-intercept points ($\Delta X,Y = 0$) were obtained, yielding a total of eight calibration parameters. The slope value for the ***B-R*** distance components was found $k_{BR} = -0.011$ in both ΔX and ΔY, while for the ***B-G*** distances $k_{BG} = -0.0052$ in both ΔX and ΔY. The pixel coordinates corresponding to the points where the values of the magnitude of LCA were found minimum are $(m_{BR}, n_{BR}) = (1051, 677)$ px for the ***B-R*** pair and $(m_{BG}, n_{BG}) = (1079, 639)$ px for the ***B-G*** pair. The optical axis of our system does not coincide with the minimal LCA point of the captured image, simply indicating that the constituent parts of our microscope may not be radially symmetric or perfectly centered.

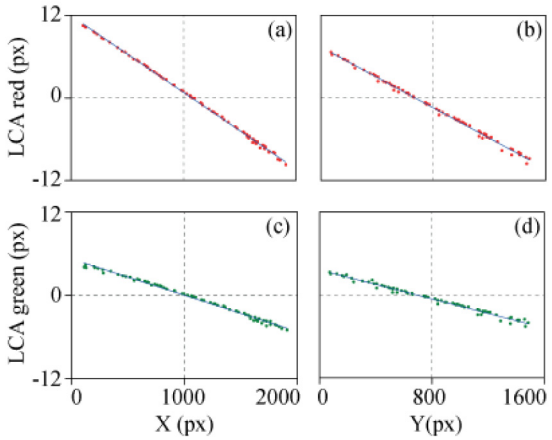

Fig. 3. Assessment of the LCA correction factors. The components (a) ΔX and (b) ΔY for ***B-R*** distances make evident a linear behavior with a negative slope of $k_{BR} = -0.011$ for both plots. In the case of (c) ΔX and (d) ΔY distances for the ***B-G*** difference, plots are also linear with a

#235180 - $15.00 USD Received 24 Feb 2015; revised 27 Apr 2015; accepted 27 Apr 2015; published 22 May 2015

slope k_{BG} = –0.0052. Dots: datapoints; lines: fittings to data. A Pearson's value of –0.99 was obtained in all cases for fits.

3.2. Correction of red and green color channels with respect to blue

Using the LCA calibration parameters previously found, an elementary image warping algorithm was carried out, according to the following:

$$I^{new}_{(m',n')} = I^{old}_{(m,n)} \tag{1}$$

$$m' = m + floor(k_{BR} \times (m - m_{BR})) \tag{2}$$

$$n' = n + floor(k_{BR} \times (n - n_{BR})), \tag{3}$$

for correction of the ***R*** channel relative to ***B***. In Eqs. (1)-(3) I^{new} and (*m', n'*) denote intensity (pixel counts) and pixel positions along (*X*,*Y*), respectively, of the new image. Similarly, I^{old} and (*m, n*) are the intensity and the pixel positions, respectively, of the original image. Here, we use the fact that the slope of the ΔX vs. X^B and ΔY vs. Y^B plots was found to be the same (k_{BR}). The conventional *floor*(*value*) function rounds the element *value* to the nearest integer less than or equal to *value*. A similar procedure is followed for correcting the ***G*** channel relative to ***B***, using the corresponding calibration parameters.

We chose to correct the ***G*** and ***R*** channels relative to ***B*** because, given the overall linear behavior and the increasing order ***R-G-B*** found for the color-dependent shifts in images, the magnitude of LCA considered (in pixels) is greater as compared to having the intermediate ***G*** channel as a reference, thus minimizing the effects of pixel digitization. Furthermore, in the correction algorithm used the calculated values of new pixel positions are rounded and truncated to integers, which can lead to missing or overrepresented pixels that tend to erode the image and affect sharpness. To reduce such unwanted effects, a bilinear interpolation algorithm was added after correction [26].

4. Experimental tests of LCA removal in bright field

As stressed earlier, digital images in bright field optical microscopy provide valuable information about image features that depend directly on color content or the pixel positions of images (such as object size, shapes and distances between objects). This information is altered in presence of LCA. Therefore, to demonstrate the effectiveness of our chromatic correction method, we evaluated different image features with the purpose to address key issues: 1) Better definition of boundaries in image elements, 2) Quantitative assessment of LCA reduction levels, 3) Faithful recording of color content, and 4) Accuracy in morphology measurements.

4.1Better definition of boundaries in image elements

We imaged a USAF 1951 test chart using white light illumination as provided by the tungsten source in the multiplexor fiber arrangement, and selected a group of black chart bars with size 87.7 μm × 17.5 μm for analysis. The original image shown in Fig. 4(a) presents a set of color bands at the bars boundaries, which in Fig. 4(d) are clearly removed after the LCA correction procedure. The unwanted color fringes are further evidenced, as horizontal and vertical intensity profiles across the bars show a misalignment between the ***R***, ***G*** and ***B*** channels, see Figs. 4(b) and 4(c). After correction, the intensity profiles for all color channels recover their alignment, see Figs. 4(e) and 4(f), resulting in improved sharpness.

4.2 Quantitative assessment of LCA reduction levels

We captured the image of a microscope calibration reticle (0.01 mm resolution) under white light illumination, and determined the location of line marks in the reticle image before and after LCA correction. In these images, we applied a similar procedure as the one described for

#235180 - $15.00 USD Received 24 Feb 2015; revised 27 Apr 2015; accepted 27 Apr 2015; published 22 May 2015

spherical particles in Section 2, to obtain the centroid coordinates (X_i,Y_i) of the line marks along the X and Y axis, see Fig. 5(a). For the X axis, the distances $d_i = X_i - X_0$ (where X_0 is a reference point) were plotted as a function of the expected d_i values. For the Y axis a similar analysis was followed. The center of the reticle pattern was selected as the reference point (X_0,Y_0). Moreover, the center of the reticle pattern was aligned to coincide with the point where the magnitude of LCA was found during the calibration procedure to be minimal for both R and G channels relative to the B channel [~(1060, 660) px]. These measures allowed us to use a single reference point in both original and corrected images.

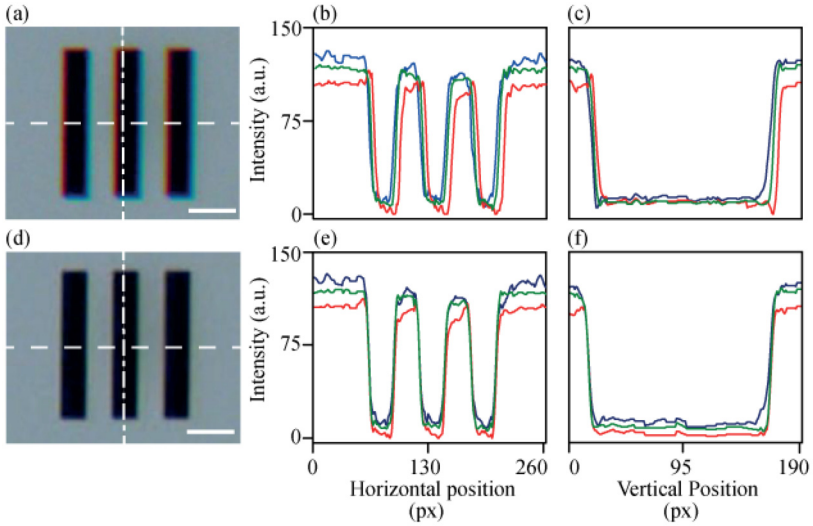

Fig. 4. Effects of LCA correction in boundaries of imaged objects. Images of a USAF 1951 test slide (a) before and (d) after LCA correction. Plots of pixel intensity of color channels across (b) horizontal and (c) vertical cross sections (whited dashed and dash-dotted lines, respectively) make evident misalignment among the color channels in the original image. The corresponding plots for (e) horizontal and (f) vertical profiles in the corrected image show that the misalignment has been removed. Scale bar: 50 px (30 μm).

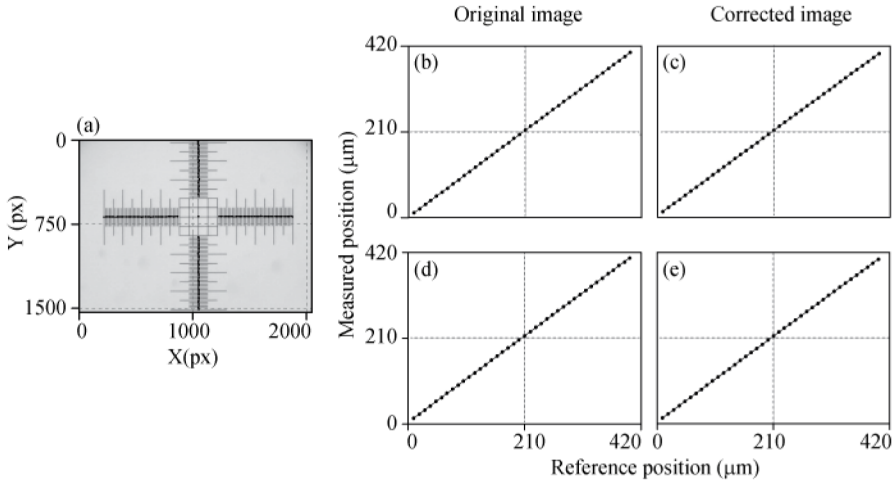

Fig. 5. Quantitative assessment of LCA after the correction procedure. A calibration slide (a) was imaged and the centroid coordinates (X_i, Y_i) of the line marks along the X and Y axis were determined. Plots show the measured line positions along (b) X and (d) Y before correction, and along (c) X and (e) Y after correction. Line fits (solid lines) to data (points) provide us with a measure of the error in position due to chromatic aberration (see text).

#235180 - $15.00 USD Received 24 Feb 2015; revised 27 Apr 2015; accepted 27 Apr 2015; published 22 May 2015

The expected distances d_i are given by the known line spacing provided by the reticle manufacturer and the pixel-to-micrometers calibration factor of our CMOS camera. The camera calibration factor was obtained by imaging a microscope reticle under blue light, to avoid the very LCA effects we want to eliminate. Finally, the slope (k) from linear fits to data points provided us with a measure of the error in position (in the ideal case the slope should be equal to 1). For the original image we obtained k_x = 1.0078, see Fig. 5(b), and k_y = 1.0071, see Fig. 5(d), whereas after LCA correction we obtained $k_{x\text{-}corr}$ = 1.0009, see Fig. 5(c), and $k_{y\text{-}corr}$ = 1.00033, see Fig. 5(e). This result indicates that the magnitude of LCA across the field of view was reduced down to the 0.1% level. In terms of distance, the magnitude of LCA averaged across the entire field of view was reduced from ~4.5 μm to ~0.5 μm.

4.3 Faithful recording of color content

We studied the impact of our LCA correction procedure in the color content of bright field optical microscopy images by means of color histograms, which are well-known representations of the number of colors present in an image. Color histograms are 3D-cartesian diagrams constructed using the information provided by the pixel intensities of the ***R***, ***G*** and ***B*** channels, where each color channel is assigned to a coordinate axis and the pixel intensity value locates a position on the corresponding axis. The intersections of these values create a color point in the coordinate system, whose tonality is calculated as a ponderation of the intensities in the ***R***, ***G*** and ***B*** channels for that pixel. Color histograms are often used in color quantization, where a range of color values is reduced to a single value, reducing or compressing the number of colors present in an image [27].

Previously, some reports on reducing LCA in optical imaging systems (mainly digital cameras) have used color histograms to display how image-processing algorithms designed to reduce LCA consistently reduce the number of colors after correction [7, 28]. However, in evaluating the effects of a procedure to remove LCA in images it would be highly desirable to compare color content between a corrected image and a reference image without LCA. To address this point, we divided the camera field of view into five zones: a central section where errors induced by LCA are small (<30% of the maximum magnitude of deviations), and four other regions surrounding the central area, see Fig. 6. A region of interest (ROI) corresponding to the central section thus served as the reference "LCA-free" image ($ROI_{LCA\text{-}free}$). Next, the sample was displaced, positioning the ROI previously identified to a peripheral section where it suffers from LCA (ROI_{LCA}). In the examples that follow, we positioned the ROI in section II, see Fig. 6. Finally, the LCA removal procedure was applied on ROI_{LCA} and its corresponding color histogram was compared to that of the unmodified $ROI_{LCA\text{-}free}$.

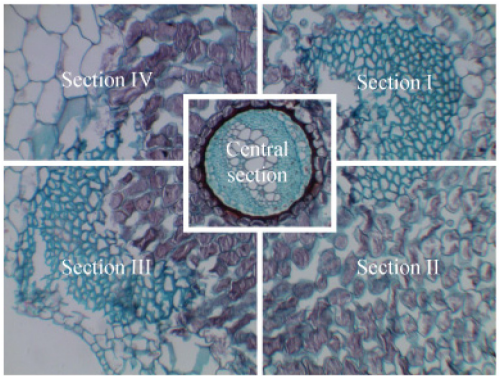

Fig. 6. Image sectioning scheme used to quantify color content before and after LCA correction, with a central section featuring minimal LCA. Field of view: 1229 μm × 921μm. The stained sample corresponds to a young yew tree.

#235180 - $15.00 USD Received 24 Feb 2015; revised 27 Apr 2015; accepted 27 Apr 2015; published 22 May 2015

Stained biological samples and a test chart were used here to evaluate color content. Results of our methodology are shown in Fig. 7, where columns 1, 2 and 3 (from left to right) display examples of images corresponding to the $ROI_{LCA\text{-}free}$, see Figs. 7(a), 7(g), and 7(m), the original ROI_{LCA}, see Figs. 7(b), 7(h), and 7(n), and the corrected ROI_{LCA}, see Figs. 7(c), 7(i), and 7(o), respectively. Below each sample image its corresponding color histogram is shown. From these views, it becomes clear that when images come from the central region their corresponding color histograms have characteristic color distributions in shape and number of colors present. These distributions are drastically modified when the ROIs are imaged in Section II, where false colors are introduced to a significant degree. Nonetheless, recovery is achieved after image correction, bringing distributions back closer to their original shape and size.

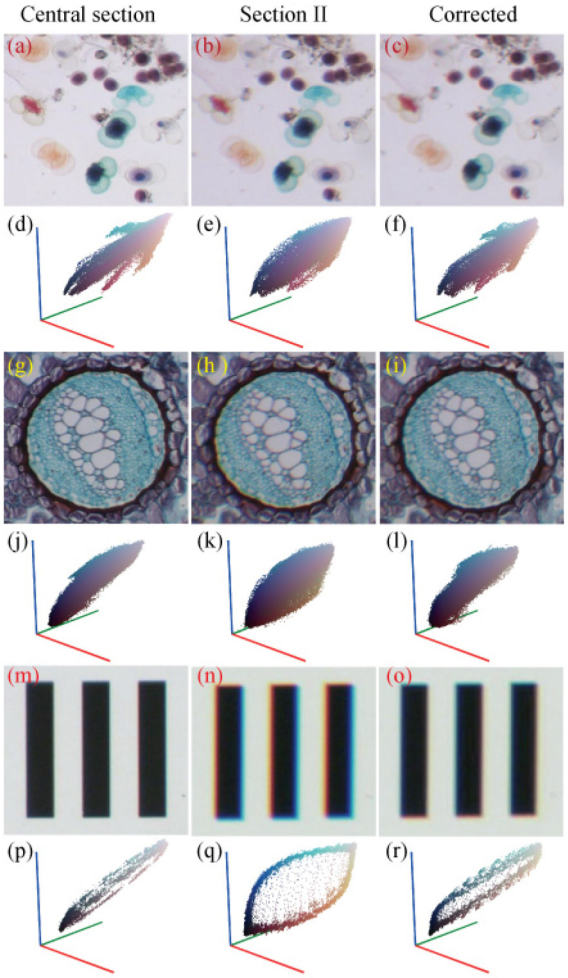

Fig. 7. Color quantization in images of biological samples of pollen grains (a)-(c), stems of young yew tree (g)-(i), and a USAF-1951 sample chart (m)-(o), and their corresponding color histograms below. The left column (a),(d),(g),(j),(m),(p) shows reference frames (corresponding to Central section in Fig. 6) and their color histograms. The center column (b),(e),(h),(k),(n),(q) displays LCA-affected frames (corresponding to Section II in Fig. 6) and their color histograms. The right column (c),(f),(i),(l),(o),(r) displays the LCA-affected frames after correction and their color histograms. Field of view: (a)-(c) 241 µm × 256 µm, (g)-(i) 356 µm × 356 µm, (m)-(o) 146 µm × 146 µm.

#235180 - $15.00 USD Received 24 Feb 2015; revised 27 Apr 2015; accepted 27 Apr 2015; published 22 May 2015

4.4 Accuracy in morphology measurements

Typical methods for automated object segmentation demand optimal definition of morphology and boundaries in addition to color consistency [18]. Such requirements are negatively altered by LCA and consequently the segmentation process is expected to improve in LCA-corrected images. We show this effect by imaging a sample of pollen grains and analyzing specimen shape. Both the original, see Fig. 8(a), and the corrected image, see Fig. 8(d), were processed with the following classification procedure: (*a*) color-based segmentation using K-means clustering [17], (*b*) application of a threshold to each resulting image, (*c*) conversion from gray scale to binary scale, (*d*) removal of image noise, and (*e*) calculation of the roundness of pollen grains. For our purposes, we have adapted the MATLAB code examples: "Granulometry of snowflakes" and "Detect and measure circular objects in an image", available in [29, 30].

We used the K-means algorithm to classify the pollen grains into two color clusters, whose members were subsequently segmented: a yellow cluster, see Figs. 8(b) and 8(e), and a dark pink cluster, see Figs. 8(c), and 8(f). It is immediately noticeable that the original image after segmentation produces image noise, see Fig. 8(b), and erosion of objects, see Fig. 8(c). In contrast, the LCA-corrected image after segmentation diminishes considerable these negative effects and the cluster classification is improved, see Figs. 8(e) and 8(f). The improvement in finding object shapes in images can be quantified by evaluating the roundness factor or compactness factor (*cf*) of pollen grains, calculated as: $cf = 4\pi A/P^2$, here A is the object area and P its perimeter.

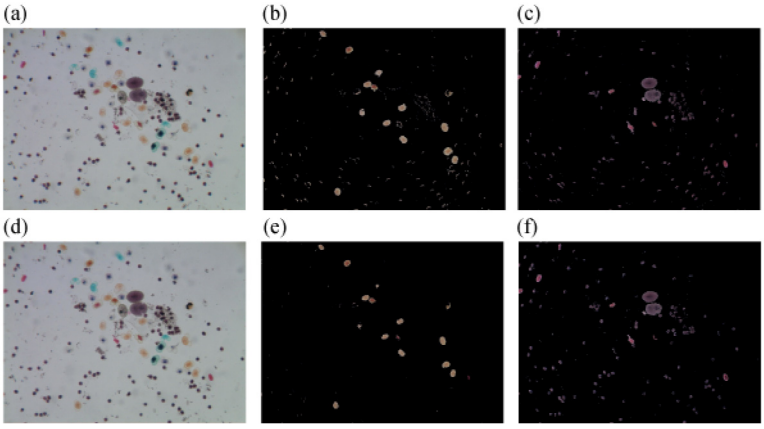

Fig. 8. Color-based segmentation in pollen grain images by K-means clustering. Top row: (a) original image, and corresponding (b) yellow cluster and (c) dark pink cluster. Clusters show high contents of noise and erosion in objects. Bottom row: (d) corrected image, and corresponding (e) yellow cluster and (f) dark pink cluster. Correction of LCA notably reduces noise and erosion in objects. Field of view: 1229 μm × 921 μm.

This factor has values that range from 0 (null roundness) to 1 (high roundness) [31]. For pollen grains, it is expected that $cf > 0.6$ [32, 33]. Analysis of the dark pink cluster in our pollen sample resulted in $cf = 0.55 \pm 0.16$ (mean ± standard deviation, mode = 0.62) for the original image, see Figs. 9(a) and 9(b), whereas in the corrected image $cf = 0.65 \pm 0.20$ (mean ± standard deviation, mode = 0.82), see Figs. 9(c) and 9(d). Therefore, classification of objects by roundness is improved using our LCA image correction method.

#235180 - $15.00 USD Received 24 Feb 2015; revised 27 Apr 2015; accepted 27 Apr 2015; published 22 May 2015

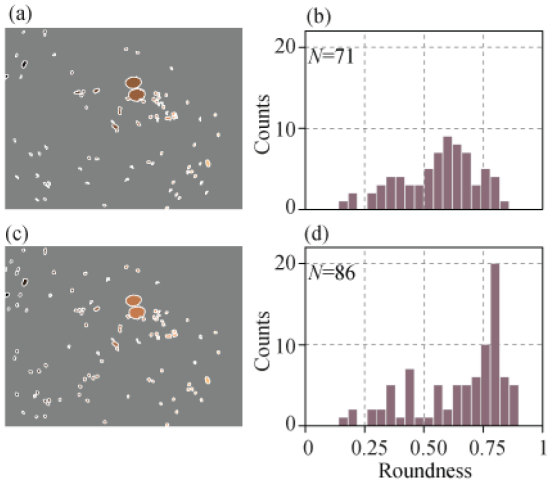

Fig. 9. Quantitative analysis of color-based segmentation results. (a) The dark pink cluster and (b) its corresponding histogram of the roundness values. (c) The dark pink cluster determined after LCA correction, and (d) its corresponding histogram of the roundness factor values. Field of view: (a), (c) 1229 μm × 921 μm.

5. Conclusions

We have reported a methodology based on sequential illumination plus digital means that removes LCA-associated errors in bright field microscopy images. In our system, we found that relative displacements among the camera color channels due to LCA had a radial distribution for both red and green channels relative to blue. A digital warping method reverted misalignments among color channels, resulting in significant reduction of errors derived from LCA. Our strategy was validated by assessing the shapes, distances, and distribution of colors in images before and after correction. Altogether, our procedure constitutes an efficient tool for quantitative image improvement in optical microscopy. Further work could explore the possibility to correct not only lateral but axial chromatic aberration as well. Similarly, the effects of chromatic aberration on object size (not only displacement) at different illumination wavelengths can be addressed.

Acknowledgments

We thank members of the Gutiérrez-Medina lab for helpful comments on the manuscript. This work was supported by grant Fondos Sectoriales-SEP-2009 (CB-2009/133053) from Consejo Nacional de Ciencia y Tecnología (CONACYT, México) to B.G-M.

#235180 - $15.00 USD Received 24 Feb 2015; revised 27 Apr 2015; accepted 27 Apr 2015; published 22 May 2015